A novel biomimetic design of a 3D vascular structure for self-healing in cementitious materials using Murray's Law

Zijing Li *, Lívia Ribeiro de Souza, Chrysoula Litina, Athina E. Markaki, Abir Al-Tabbaa

Department of Engineering, University of Cambridge, Trumpington Road, Cambridge CB2 1PZ, UK

*Corresponding Author

Email: zl380@cam.ac.uk

Phone: +44 7802706975

Submitted: October, 2019

Revised: February 2020

Abstract:

Nature has always been a source of inspiration in engineering applications and vascular networks, as in human skin and in a tree leaf, are one attribute that has received attention in the design of resilient structures. A vascular system houses healing agents within its hollow channels or interconnected networks which are incorporated within a cement matrix. It is the only self-healing approach that has the capability to address different scales of damage in cementitious materials. The main aim of this work is to develop a novel vascular network inspired by nature for self-healing in cementitious systems. To achieve this, a biomimetic three-dimensional (3D) vascular network was designed and generated following Murray's Law for circulatory blood volume transfer. The designed structures were constructed through 3D printing and assessed in a cement-based matrix. One-dimensional (1D) and two-dimensional (2D) models were also designed, printed and embedded into cement prisms to compare with the 3D vascular system. Load recovery was used to assess recovery in mechanical properties after the sample was cracked and pumped with sodium silicate for 28 days. Mechanical testing assessed the compatibility of the system with the surrounding matrix as well as the functionality of the network in delivering and releasing the healing agent at the location of damage. This initial proof of concept work confirmed the ability of all vascular systems to deliver the healing agent after a damage event, and the 3D vascular system demonstrated a significantly enhanced healing performance.

Keywords: Vascular networks, Biomimetic structures, 3D printing, Self-healing, cementitious materials

Highlights

- 3D printed structures presented brittle fractural response and suitable interfacial bond for mechanical triggering.
- The increased load applied to crack the samples with embedded 1D, 2D and 3D vascular network indicated that the plastic tube acted as reinforcement of the cement beams.
- The vascular network was effective in delivering the pumped sodium silicate

as healing agent for 28 days in the three systems. Initial cracks (between 700 to 800 μm) from all systems were observed to be healed after 28 days.

- The healed crack volume indicated partial healing could be drastically reduced by applying a 3D vascular structure, which contains more connected daughter tubes and enables large tube coverage.

1. Introduction

Nature has always been a source of inspiration for ideas in addressing engineering materials challenges given that natural materials can be flexible, strong and lightweight and many are able to self-heal (Wegst et al., 2014). Natural vascular systems have been an inspiration in the development of self-healing systems in polymer-based composites and more recently cement-based infrastructure and construction material systems (Williams et al., 2008).

Cement-based infrastructure materials have limited intrinsic ability to heal very small cracks (0.15 μm) through a combination of continued hydration and carbonation processes under optimum curing conditions (De Rooij et al, 2013). To enhance the ability to self-heal larger and more complex damage, functional engineered additions have been developed cementitious systems. Encapsulation-aided healing has been one of the most popular and successful approaches based on the release of healing agents from embedded reservoirs in a range of capsules of different sizes, shapes and materials (Van Tittleboom et al, 2011, De Belie et al, 2018). Although a variety of capsules have been developed, capsule-based self-healing provides a limited amount of healing agent; this precludes the healing of larger cracks and repeated damage repair. However, this technique has difficulties in ensuring damage scenarios that require larger volumes of healing agents and repeated damage repair due to its uncertainty of capsules breaking and limitation in providing enough healing agents for large cracks (Huang et al., 2014). Alternatively, multiple local healing events can be achieved by vascular-based self-healing. With a circulation system, healing agents could be recycled and refined, which provides a way for continuous healing agent delivery.

Ideal vascular network designs should consider blockages and avoid weakening the matrix while increasing vessel coverage (Heywood, 2015). Initial tests with vascular systems investigated 1D-systems fabricated with hollow glass tubes containing healing agents offer a simple path for application of vascular network (Dry 1994; Joseph et al., 2010; Thao, 2011; Kanellopoulos et al, 2015). However, unwanted blockage due to the reactivity of the healing agent may obstruct the flow of the healing agent. 1D-systems fabricated with hollow glass tubes containing healing agents such as methyl methacrylate and cyanoacrylate form solidified products before delivery; this leads to the formation of solid products inside the vascular system and consequently, no healing agent is delivered. (Van Tittleboom et al, 2013) This limitation can be mitigated by using 2D-systems, as it provides extensive redundancy of flow paths to maintain supply to the critical region (Williams et al., 2008). Polymers, such as PLA, can be used for 3D printing the tubes (Heywood, 2015) or the connections (Davies et al, 2015). However, this approach only provides healing agents in one plane of the composite, limiting the coverage of healing agents and thus diminishing or compromising self-healing performance. Maximum volume coverage with vascular networks can be achieved with 3D gridded channels (Davies et al, 2015). The resultant dense connected network provides redundancy for blockage and

increase vessel coverage. However, the increase in vessel density may affect the mechanical properties of the sample and blockage become the main concern in rectangular bend tunnels (Williams et al., 2008; Heywood, 2015).

To minimize turbulent flow at junctions while also maximizing the volume, researchers such as Justin et al. (2016) investigated a biomimetic vessel structure in cellularized hydrogels via stereolithography printing technique following Murray's Law. Kimber (2014) investigated a bio-inspired 3D vascular network in cement pastes. The progression of the network design is shown in Figure 1G. Strength recovery was found to be 72% after a curing time of 48 hours using cyanoacrylate-based adhesives.

Specifically, for the vascular networks of blood vessels, Murray (1926a, 1926b) developed the principle of a relationship between the optimum parameters (diameter, length and splitting angle) of daughter branches and parent branches in order to minimise work required for blood transport. The law states that when a parent blood vessel branches into daughter vessels, the cube of the radius of the parent vessel is equal to the sum of the cubes of the radii of daughter blood vessels. This provides inspirations for designing interconnected networks in self-healing cementitious materials.

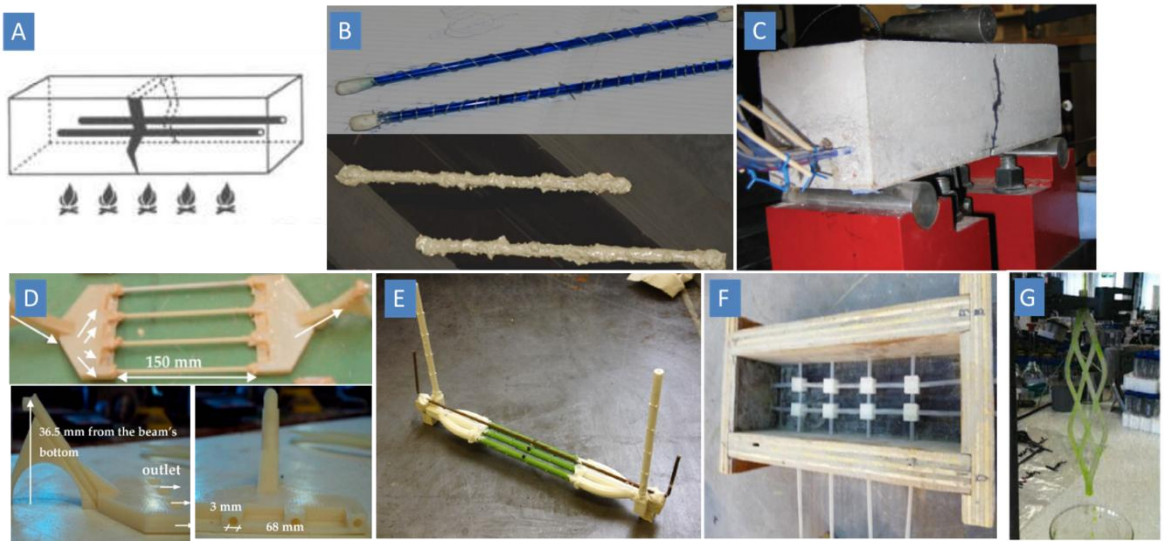

Figure 1. Examples of 1D (A-C) and 2D (D-F) cementitious vascular systems investigated (A) Wax coated 1D vascular system (Dry, 1994), (B) glass tubes with protective spiral wire coated with 3.5 mm-thick mortar layer (Thao, 2011)., (C) specimens with individual tubes connected to the external environment (Joseph et al., 2010), (D) 3D printed ABS distribution with individual inorganic phosphate cement (IPC) tubes (Minnebo et al., 2017), (E) layout of a 2D network printed by PLA and ABS (Heywood, 2015), (F) 2D gridded polyurethane network with PLA connections (Davis et al., 2015), (G) Individual 3D network fabricated by PLA (Kimber, 2014)

In this study, we design and fabricate a 3D-vascular network inspired by biomimetic design following Murray's law that shows broadened coverage of healing agent distribution. The biomimetic three-dimensional design was 3D-printed using polylactic acid (PLA) for the production of the vascular network and compared with corresponding 1D and 2D networks for use in self-healing of cementitious materials. We show the PLA structures presented brittle fractural response and suitable interfacial bond for mechanical triggering. In addition, the increased load applied to crack the samples with embedded 1D, 2D, and 3D vascular network indicated that the plastic tube acted as a reinforcement of the cement beams. We demonstrate the vascular network was effective in delivering the pumped sodium silicate as a healing agent for 28 days in the three systems. Initial cracks (between 700 to 800 μm) from all systems were observed to be healed after 28 days. A recovery in mechanical properties, reduction in sorptivity, crack mouth closure and healed volume were used to assess the self-healing performance of the systems embedded with a 1D, 2D, and 3D vascular network. Biomimetic design obeying Murray's law have great future potential for delivering healing agent for self-healing and the investigation could be expanded to other healing agents.

2. Materials and Methods

2.1 Cementitious mixes and prisms

Prismatic specimens were prepared for testing the viability of the 3D printed vasculature within the cement matrix. The cement paste mix prepared using Ordinary Portland Cement (PC) (CEM-I, 52.5, supplied by Hanson) and water in a 0.4:1 ratio by weight. Printed tubes were held by iron support stands to maintain their position in the moulds before and after pouring the cement mix. Cement mix was then poured into the stainless-steel moulds (80 mm × 80 mm × 300 mm) and vibrated at each stage to remove the air bubbles. Samples were submerged in water to cure for 28 days. Thin steel wires (Ø1.25mm; Top margin, 35 mm; left & right margin, 15 mm; shown in Figure 2) were used to simulate the cover placement of the network and to prevent complete failure of the prism upon cracking. Three prisms were prepared for each vascular network system. Sodium silicate (SS) was chosen as a healing agent for its chemical compatibility with the cementitious matrix and for having a slower reaction process (Kanellopoulos et al., 2015; Alghamri et al., 2016).

The vascular networks were designed in Creo® and then printed by polylactic acid (PLA) via an Ultimaker® 3D-printer together with Cura® software. Due to the size limitation of the 3D printer, each vascular structure was printed as two parts before being soldered together. Kimber (2014) and Heywood (2015) showed the ideal size of the minimum scale tubes, with a 2 mm inner radius, would have a relatively more effective geometry and good performance in avoiding printing errors. This is because speed variation of the 3D printer tool, errors in the positioning systems, fluctuation of temperature and non-uniform flow can cause anomalies in the parts that can affect the local error (Oropallo and Pieg, 2016; Günaydın, 2018), resulting in extruding unexpected parts or blocking printed tubes with small diameters.

2.2 Characterisation methods

The morphology of the crack opening development was observed via a GXCAM-1.3 microscope and Celestron® portable microscope together with GXCapture® software. Images of initial cracks were captured after loading to obtain the reference crack widths. The microstructures of the hydrated cement, mineral, and self-healing products were investigated with SEM-EDX using Phenom (Pro G2, Netherlands). Electron beam energy of 15 keV with a short working distance (~6-8mm) was used for all imaging. Samples were coated with gold film (2-3 nm) using a K550 Emitech coating machine to ensure decent conductivity and signals in microscopy and EDX. Cement beams were scanned at Nikon on an X-Tek H 225 ST CT-scanner. Reconstruction of the original CT images produced 1300 slices (oriented obliquely through the specimen) composed of isometric voxels with a resolution of 0.089579 mm/voxel; CT scans were processed using the 3D visualisation software package Mimics v.14.0 (Materialise HQ, Leuven, Belgium).

2.3 Loading and testing

A four-point bending test, conforming to ASTM Standard D6272-02, was applied to the prisms 28 days after casting. The prisms were placed on two steel supports with a span of 240 mm and the upper surface of the beams was loaded through two steel rods (50 mm in diameter) with a span of 120 mm (schematic in Figure 2). Vascular structures were centred (Top margin, 30 mm; left & right margin, 20 mm; shown in Figure 2;), leaving 40 mm of 'L' shaped artery tubes outside for connecting the external pumping system. The printing layers of the PLA tubes were in parallel with the crack plane to ensure successful physical trigger (Zhou et al., 2018). An Instron® 5500R-150kN testing frame was used with a quasi-static displacement controlled rate of 0.25mm/min, then this process stopped when the amount of load dropped more than 40% compared with its previous figure. The same loading program and span set-up were applied in both 3D printed vascular structures (structures only, no healing agents added) and cement specimens.

Evaluation of specimens' water tightness (before and after healing) was examined by the capillary water absorption test, following ASTM C1585 (ASTM C1585 2013) and RILEM report (De Rooij et al., 2013). The beams were first dried in a vacuum chamber (25°C) until the mass changes were less than 0.1% between 24 h periods. The specimens were then wrapped on the bottom and lateral dies with aluminium tape but the crack area was left uncovered for exposure to capillary water suction. During the sorptivity test, specimens were immersed in distilled water at a depth of 5 ± 1 mm.

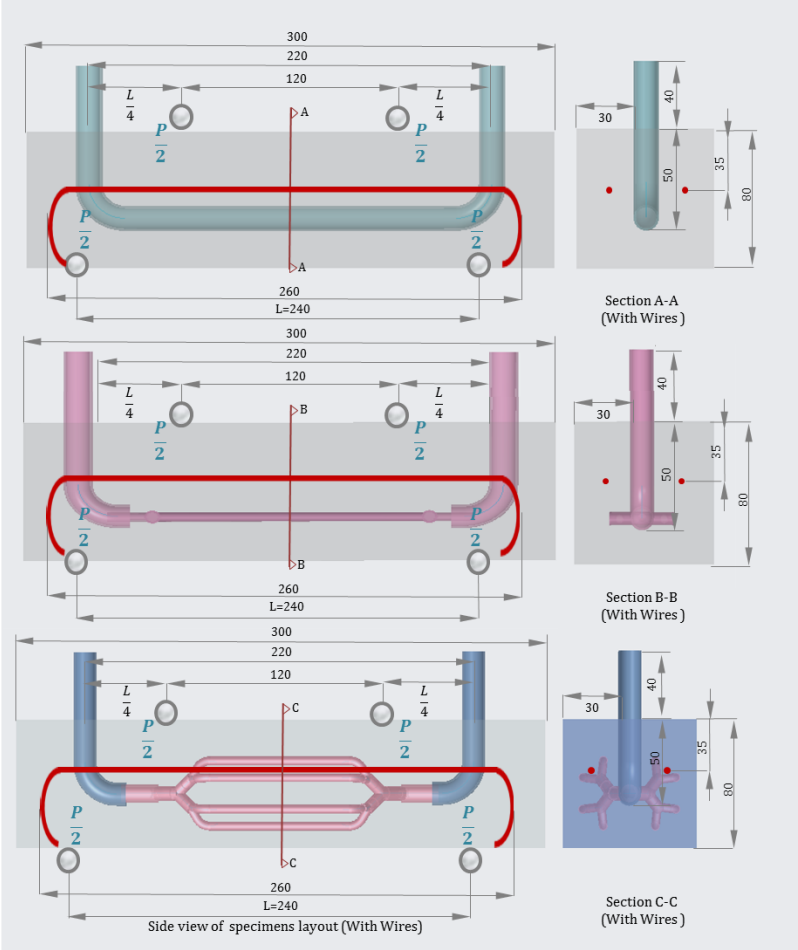

Figure 2 A schematic of the experimental setup for the four-point bending of specimens with the different internal vascular structures (a) 1D system, (b) 2D system and (c) 3D system

After the cracks were initiated, the artery tubes left outside were linked with external silicone tubes connecting the pump and healing agent reservoir, Figure 3 B. The healing agent migrated out from healing agent reservoir, then into the pump before being driven into the cracked beams. Healing agent was then pumped through the beam and recycled back to the healing agent reservoir. Healing agent released from cracks was also collected and recycled back to the reservoir.

The water absorption was evaluated by measuring the mass changes of the specimens at different time up to 256 minutes, and normalised by the surface area (80 × 20 mm^2) and the density of water (1 × 10^{-3} g/mm^3), as shown in Equation 2.1, 2.2 (Hall & Tse, 1986):

$$M_w = \frac{\Delta m}{A \cdot \rho} \quad (2.1)$$

$$M_w = \mathrm{C} + \mathrm{S}\sqrt{t} \quad (2.2)$$

where M_w is the water uptake quantity uptake per unit area of inflow surface (mm); Δm is the mass changes of specimens (g) during water absorption; A is the

inflow area; ρ is water density (g/mm^3); S is sorptivity coefficient (mm/h$^{1/2}$) determined by the slope of $M_w - \sqrt{t}$ curve.

To compare the channel resistance difference in 1D/2D/3D structure, the engineered vascular matrix is connected to a recycling system for measuring the pressure changes, consisting of a peristalsis pump (Watson Marlow 323, providing consistent pumping rate 60 mL/min), a reservoir (containing 500 mL sodium silicate), two pressure transducers (RS Components, 249-3864, 1bar, 0-100mV), and connection tubing. Resistance of the designed 1D/2D/3D vascular systems was then calculated according to Akers (2006) and Choi et al., (2010), which the laminar incompressible flow of steady-state inside a channel is described by:

$$Q = \frac{\Delta P}{R} \quad (2.3)$$

where Q (mL/s) is the volumetric flow rate, ΔP (kPa) is the pressure drop from one end of the channel to the other, and R (kPa • s • mL^{-1}) is the hydraulic resistance of the channel.

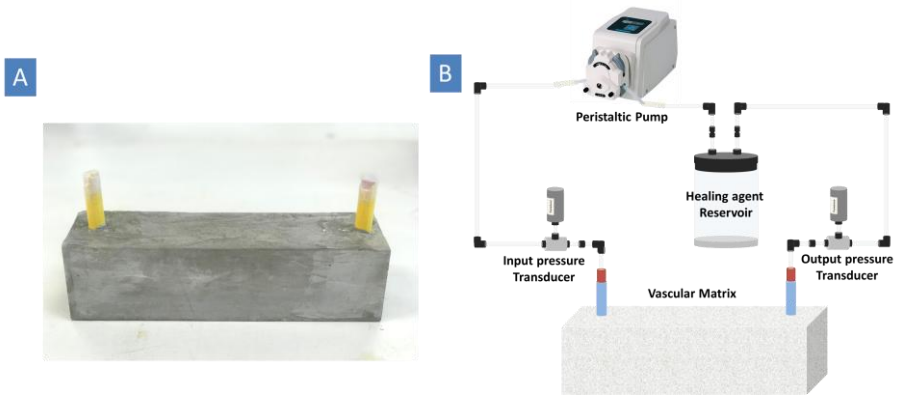

Figure 3 A, sample specimen with vascular network; B, schematic set-ups for measuring the pressure changes of the vascular system

3. Results and Discussion

3.1 Design of vascular networks and their behaviour in cement

The biomimetic design aims to (i) increase vessel coverage; (ii) avoid weakening the cement matrix; (iii) ensure strong bonding between the walls and cementitious materials (iv)avoid blockage while the healing agent pumped throughout the system, thereby achieving rapid physical triggering response and effective healing process Furthermore, the printed structure should be strongly bonded with the cementitious matrix to assure successful Physical triggering of the tubes.

As a result, a branch-like distribution of the healing agent is achieved while minimising the space occupied by the vascular network and preventing blockages in junction areas. When Murray's law is considered, three main aspects are important: the optimal diameter, length and angle relationship between the daughter and parent branches (Murray 1926a, b). A schematic representation of the vascular network and its main parameters is presented in Figure 4.

We consider a cylindrical tube, highlighted in yellow in Figure 4C, where the diameter is D and length is L. Based on a fluid-dynamic interpretation, for energy to be minimised, the sum of the energy used to overcome friction due to shear stress (Rodbard, 1975) on the walls.

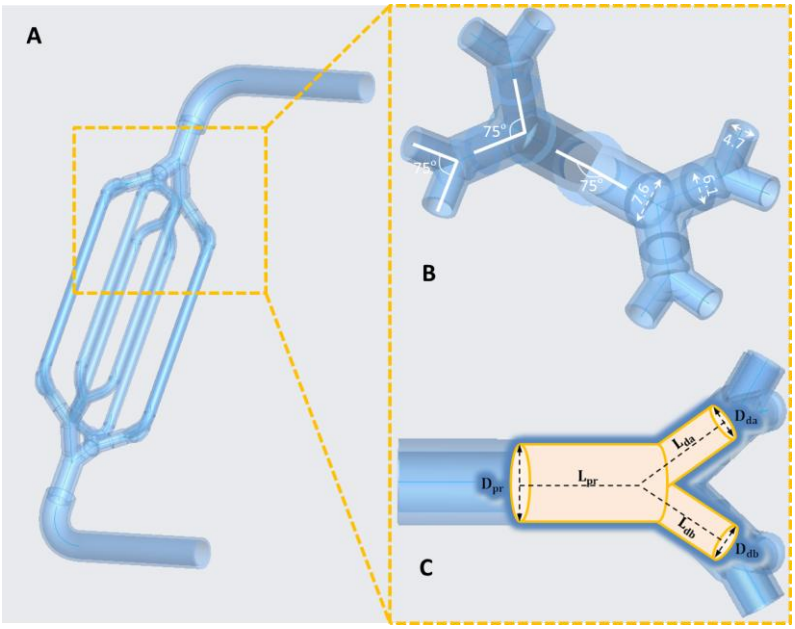

Figure 4 A biomimetic design of 3D vascular network; (A) designed model following Murray's law; (B) parameters considered in the model; (C) fluid dynamic diagram adapted in this model.

Similar to electricity, the total flow resistance of the tubes is explained in equation 3.1, where R_{pr} (resistance of parent branch) and R_{da} (resistance of daughter branch a) and R_{db} (resistance of daughter branch b):

$$R_{h,Total} = R_{\mathrm{pr}} + \left(\frac{1}{R_{da}} + \frac{1}{R_{db}}\right)^{-1} \quad (3.1)$$

Considering a symmetrical system with 2-branches, all the daughter branches diameter, D_{dg}, are the same, so $D_{da} = D_{db} = D_{dg}$. The same applies to the length Ldg, where $L_{da} = L_{db} = L_{dg}$. Thus $R_{h,Total} = R_{pr} + \left(\frac{2}{R_{dg}}\right)^{-1}$. In order to find the relationship between the length (L) of daughter branches and parent branches, the flow resistance R_h is represented by D and L based on fluid dynamic interpretation as shown below (equation 3.2, Miguel, 2016):

$$R_h = \frac{\Delta p}{Q^{\omega}} = \frac{4M[8\left(\frac{1}{\omega} + 3\right)]^{\omega} L}{\pi^{\omega} D^{3\omega+1}} \quad (3.2)$$

where Δp is times the pressure drop, Q ($Q = \frac{\pi D^3}{8(\frac{1}{\omega}+3)} \left(\frac{D}{4M}\frac{\Delta p}{L}\right)^{\frac{1}{\omega}}$) is volumetric flow rate and defined as the product of axial velocity and the cross sectional area of the tube, ω is the fluid behaviour index (or the power-law exponent) and M is the fluid consistency index (represents viscosity). By considering constructal law

(Bejan, 1996), maximising flow access means minimising resistance under constrains. In the pursuit of achieving local minimum resistance, the boundary condition is given by $\partial R_h / \partial D_{pr} = 0$. So that the relationship of diameter in this symmetric branching system is given by:

$$\frac{D_{Daughter}}{D_{parent}} = 2^{\frac{-2}{3\omega+3}} \quad (3.3)$$

And the relationship of length in this symmetric branching system is given by:

$$\frac{L_{Daughter}}{L_{parent}} = 2^{\frac{-3\omega+1}{3\omega+3}} \quad (3.4)$$

Sodium silicate was used as a model mineral healing agent for this study, as its reactions with the cementitious matrix can recover the mechanical strength. As sodium silicate is a Newtonian liquid, ω=1 and Equation 3.3 and 3.4 yields $\frac{D_{Daughter}}{D_{parent}} = 2^{\frac{-1}{3}}$ and $\frac{L_{Daughter}}{L_{parent}} = 2^{\frac{-1}{3}}$. Detailed figures for vascular dimensions could be found in Figure 4 B. The artery connecting the pump to the fitting was limited to the pump tubing and defined as 13.6 mm outer diameter (OD) and 11.6 mm inner diameter (ID). Then, the first parent branch was adapted to 11.6mm OD and 9.6 mm ID in order to fit snug in the artery. Thus the daughter branches ID were calculated from Equation 3.3 as 7.6, 6.1 and 4.7 mm, as shown in Figure 4 B. Formia et al. (2015) found that viscous healing agents, such as sodium silicate cannot be released from the tube smaller than 2 mm in diameter. In addition, for viscous liquids, the pressure cannot be increased more than 7250 psi in PLA tubes, which is the maximum tensile strength of PLA material. Considering this, the minimum inner diameter of the daughter branches was 4.7 mm and was sufficient enough for delivering sodium silicate for this study.

Murray also provided an original formula for the angle of branching, giving the idea of treating non-symmetric branches and trifurcations (Equation 3.5 and 3.6). According to Murray (1926b), the correlation between the branching angle and the radius ratios should be:

$$cos\alpha_1 = \frac{r_0^4 + r_1^4 - (r_0^3 - r_1^3)^{\frac{4}{3}}}{2r_0^2 r_1^2} \quad (3.5)$$

$$cos\alpha_2 = \frac{r_0^4 + r_2^4 - (r_0^3 - r_2^3)^{\frac{4}{3}}}{2r_0^2 r_2^2} \quad (3.6)$$

Due to symmetric splitting for this design:

$$cos\alpha_1 = cos\alpha_2 = \frac{1 + \delta_1^4 - (1 - \delta_1^3)^{\frac{4}{3}}}{2\delta_1^2} \quad (3.7)$$

In this case, $\delta_1 = \frac{1}{\sqrt[3]{2}}$ (3.8)

Which provides $\alpha_1 = \alpha_2 = 37.5^\circ$.

In addition, the design of the length for each generation daughter branch was limited by angle (3.8), length relationship (3.4) and cement beam parameters (length 300mm, width or height 80 mm). Then, the first parent branch was adapted to 26.0 mm. Thus the daughter branches were calculated from Equation 3.3 as 20.6, 16.3 and 12.9 mm.

A biomimetic 3D vascular network was fabricated together with a single tube 1D structure and a 2D network connected to 4 longitudinal tubes. An inner/outer diameter ratio of 0.83 was applied in all vascular structures (1D/2D/3D) for further comparison.

In Figure 5, both designed (Figure 5 A, B & C) and final fabricated structures (Figure 5 D, E & F) were presented. The arrows indicated the sodium silicate flow through the systems. A volume of 65 ml was designed for all 1D/2D/3D structures to control the same amount of healing agents passing through during healing process. The volume of each fabricated structure had been further measured and confirmed by connecting the printed structures with a scaled container.

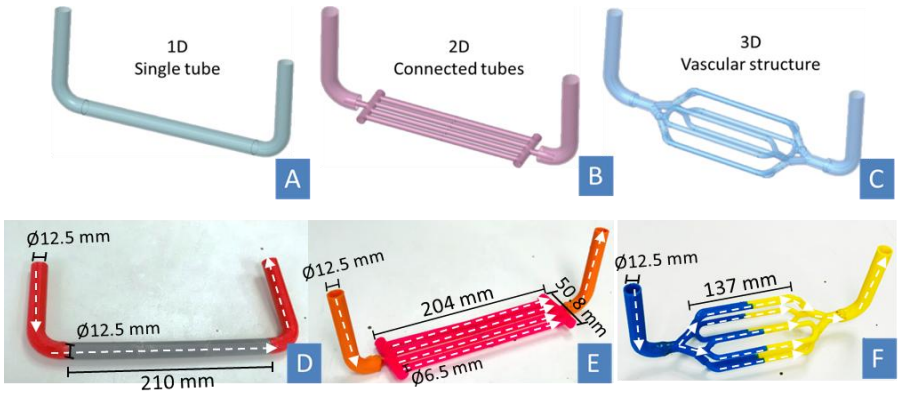

Figure 5, Designing model of 1D/2D/3D structures (A, B, C) and front view of final manufactured structures (D, E, F)

Fractural response of 3D printed structures was also examined before being embedded into cement, as shown in Figure 6 A. Structures were loaded to failure during the tests. Five parallel tests were carried out in each vascular type, to avoid accidental error. Results showed that single tube (1D structure) received the lowest loading, at around 71 N. 2D and 3D on the other hand, had relatively higher figure, at 129 N and 134 N respectively. 2D and 3D networks demonstrated higher load response than 1D structure, as they have more supporting structures to distribute forces rather than concentrating on one single tube. Similarly, Heywood (2015) reported that a thinner (with 4 mm inner diameter and 5mm outer diameter, 188mm in length) single PLA tube failed at 27.5 N during test (loading rate 0.125 mm/min). This is much lower than the 1D structure (with 12.5 mm inner diameter and 15 mm outer diameter, 210 mm in length) in our study. Loading response difference relates with loading rate, bending methods (three points, four points), and the tube thickness in this case. Thickness of the tube was one of the main reasons that resulted in different

load response for a single tube, as the same commercial PLA was used for printing. As a result, all 3D printed PLA structures failed below 150N, which indicated that they required low energy to crack and release healing agent, making 3D printed PLA structure an ideal option for self-healing structures.

There was around 2.5 kPa pressure difference in 1D system, which correlated its total resistance was 2.5 kPa • s • mL^{-1}(Figure 6 B). In 2D system, secondary channels were designed with 90-degree branching angle. The figures for both pressure change and resistance increased to approximately 7.6 kPa and 7.6 kPa • s • mL^{-1}. The channel complexity, cross-sectional areas and branching angles can affect the growth of hydraulic resistance (Razavi et al., 2014). In the case of 3D structure, hydraulic resistance was only 2.9 kPa • s • mL^{-1}. It was demonstrated that fluidic channels which obey Murray's law improve fluidic control (Lim et al., 2003).

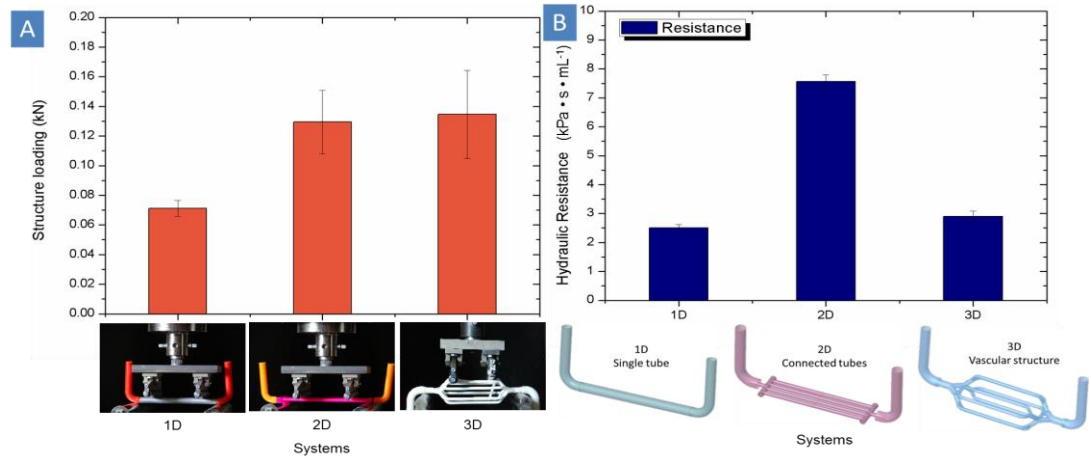

Figure 6, Load response of 1D/2D/3D printed structures, combining with photographs during loading process (A); and hydraulic resistance of 1D/2D/3D models (B)

3D printed pattern on the tubes provided a rough surface compared with smooth PU tubes applied in Davis et al (2015), which could be easily pulled out after cement beam were cured. The pattern increased friction between 3D printed structures and cement matrix (Figure 7). As shown in Figure 7 C, 3D printed tubes clearly remained their pattern on cement pastes, which created a rough surface on the cement side and thus enhanced the bonding between vascular structures and cement beams.

All different 3D printed structures did not debond from the cementitious matrix confirming the strong adhesion between them and the brittleness of PLA which enabled its fracture. This means 3D printing patterns and PLA materials are suitable for producing vascular structures and are bonded well with cement specimens.

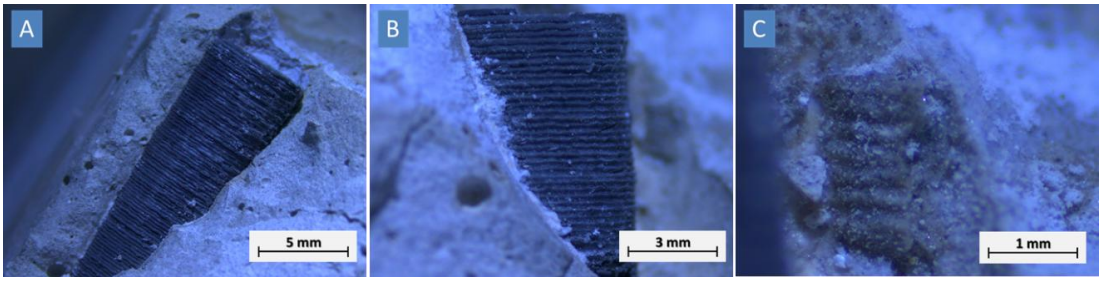

Figure 7, microscope image of the connection between individual tube and cement beams, boundary between vascular structures and cement matrix (A); minerals between PLA tube and cement matrix (B); pattern remained after tube was manually separated from cement (C)

3.2 Assessment of mechanical property recovery

Loading recovery after healing was used to evaluate the mechanical triggering and healing efficiency of the vascular system. Four-point bending tests were applied to form unexpected cracks in the samples embedded with the fabricated 1D, 2D and 3D vascular networks and the results are shown in Figure 8. Plain cement beams showed the least load response, at around 5kN. The load increased to 6kN when the wires were added. An increased load was necessary to crack the samples embedded with the vascular networks once compared with the control sample (Figure 8 A), hinting the physical triggering or the PLA tubes. In addition, the increased load applied to crack the 1D, 2D and 3D vascular network indicates the plastic tube acts as reinforcement of the cement beams (Kim and Han, 2017)), as the plastic structure served as a medium for the transfer of stress between the cement matrices (Yuhazri et al., 2017). After the crack was formed, there was no healing agent pumped in during curing process. Autogenous healing was observed in the controlled beams, which received an approximately 3% of loading recovery. For the treatment groups, sodium silicate solution was pumped into the systems continuously for 28 days at 60 mL/min. Load recovery of ~20% was observed for 1D and 2D-structures while 3D vascular network specimens reached 34%, compared with the initial loading. A previous investigation of self-healing performance using sodium silicate encapsulate in in glass vials reveals similar results to the 1D and 2D-systems, with load recovery rate of 20–25% (Kanellopoulos et al., 2015). The increased load recovery of the 3D vascular network was attributed to delivery of healing agent at multiple points at the surface of the crack, thus enhancing the healed surface.

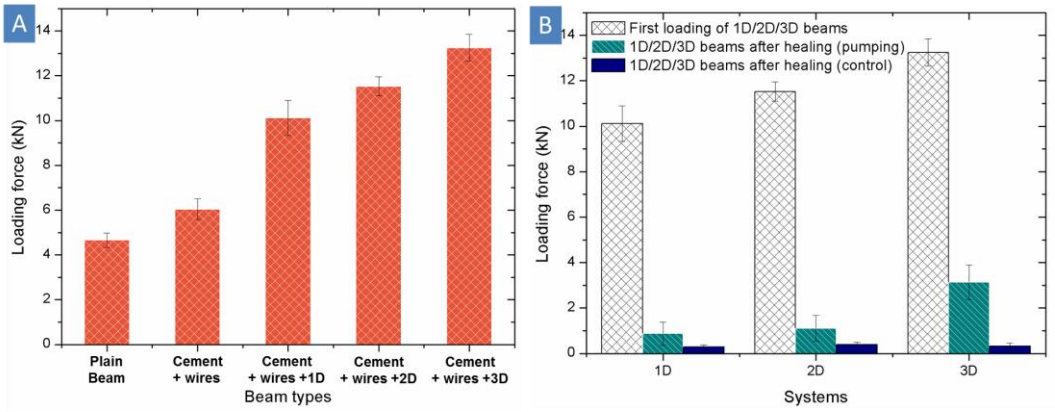

Figure 8, Vascular-cement systems loading response; (A)loading response of plain cement beam, beam with wire holders, beam with holders and vascular structures; (B) loading forces of 1D/2D/3D vascular structures and vascular-cement systems before and after healing; The results presented here are the average from 3 tests and the error bar signifies the standard deviation.

3.3 Assessment of transport property recovery

To evaluate the recovery in water tightness, the capillary water absorption for the cracked concrete specimens with and without healing was also measured. The durability of concrete depends predominantly on the ease with which fluids enter and move through the matrix and sorptivity is an indicator of concrete's ability to absorb and transmit liquid through it by capillary suction. Figure 9 plots the water uptake process and the capillary water absorption through the crack before healing (A, B), and after 28 days of pumping (E, F) and not pumping (C, D) sodium silicate. No significant difference in the water uptake was observed for the control samples compared with the samples before healing (Figure 9 A and C). The results indicate that autogenous healing in air condition barely contributed to enhance the water tightness. Besides, the 1D/2D/3D network did not provide any preferential flow path in cement. Figure 8 E shows the water uptake after healing, where the preferential water flow path is blocked by the healing products, and the water absorption by capillary action and the overall sorptivity is reduced. The mean sorptivity coefficient values for the 1D/2D/3D vascular-cement of cracked samples before healing are 12, 13 and 13 ($mm/h^{1/2}$) and 9, 4 and 3 ($mm/h^{1/2}$) after healing. Thus, the reduction ratio of initial sorptivity is 25, 69 and 77% for the 1D, 2D and 3D vascular-cement, respectively. This is because capillary flow within cracks is mainly influenced by crack width and depth. When solidified sodium silicate gel blocked the crack, the crack length and depth were shortened, thereby slowing down water uptake (Alghamri et al., 2016) and then reducing water sorptivity. In this case, 3D vascular system was able to block more crack area compared with the 1D and 2D systems.

Figure 9 shows the changes in the water absorption of the three vascular beams over time before and after healing. As shown in Figure 9 B and D, the water absorption in all specimens was proportional to the square root of time after 1 h. The reason of choosing data for linear analysis after 1h is because (1) water uptake at early stage could be affected by the accuracy while measuring in a short time of period; (2) few unstable sodium silicate gel would be dissolved by water at early stage. From the slope of the graph of water absorption vs square root of time, and is calculated using Equation (2.1, 2.2).

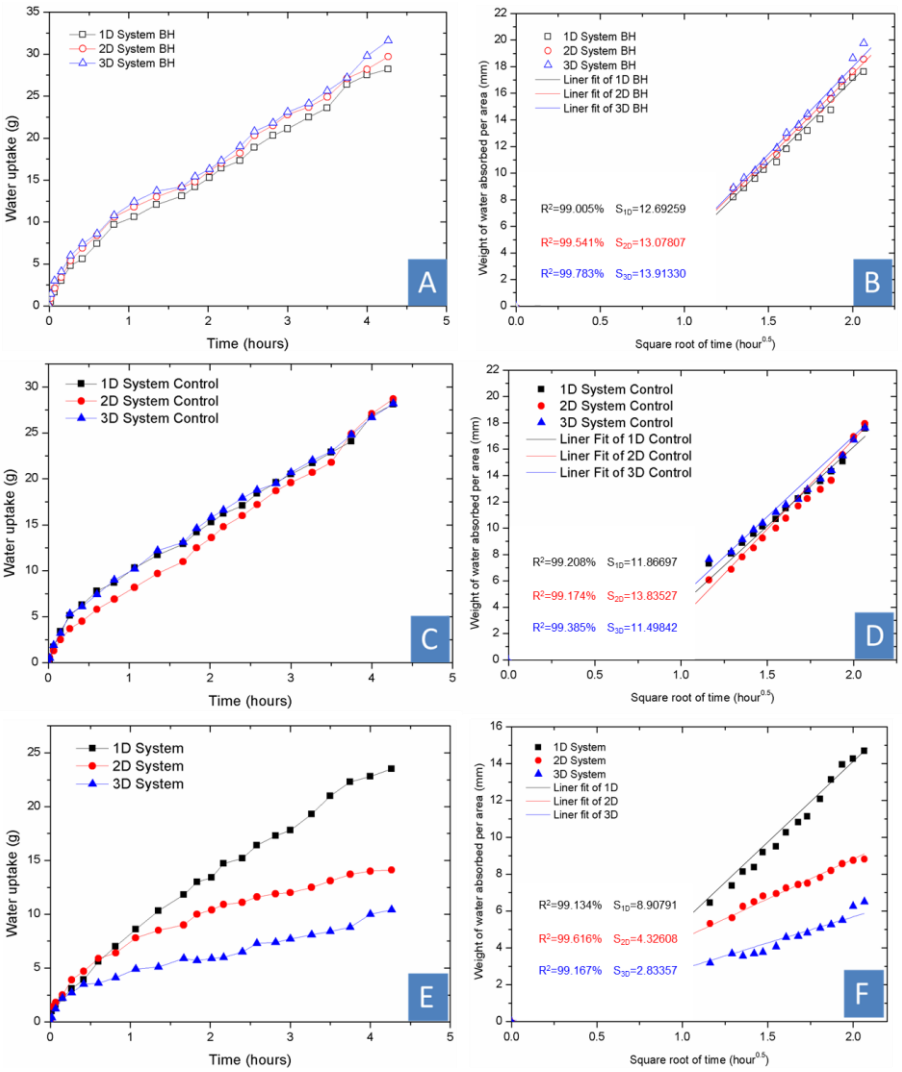

Figure 9. Water uptake process over time before healing (A), control group (without healing agent pumping) after healing (C), and treatment group (with healing agent pumping) after healing (E); Water sorptivity of specimens vs the square root of time before healing (B), control group after healing (D) and treatment group after healing (F).

3.4 Crack closure and healing materials

In addition to showing recovery in mechanical and transport properties, the surface crack area also decreased as time went on for the 1D/2D/3D vascular-cement systems. Optical microscopy was used to quantify the initial crack width and the final crack closure after healing. The four-point bending test was set to stop after the load dropped more than 40%, thus resulting in the widest part for each crack in the range between 700 and 800 μm in all vascular systems before healing. Crack location was random in between loading spans as expected since four points bending method allows for uniform force distribution between the two loading noses (Figure 10).

Crack patterns of vascular beams showed gradual type of failure. This is because holding wires will also act as a backbone to the cement beams as they tend to support the entire load of the cement and connect the crack surface so the beam does not

fracture into two sections. Shape of vascular structures did not affect the pattern significantly, and there was no specific pattern propagation trend in 1D/2D/3D beams. This can be explained by the microstructure of 3D printed PLA in Figure 7, as the layer of 3D printed PLA tube have significant gaps where the print head finishes one layer and moves on to the next. These imperfections between layers act like a crack within the material and make it far more brittle than a solid PLA tube when cracks were initiated (Heywood, 2015).

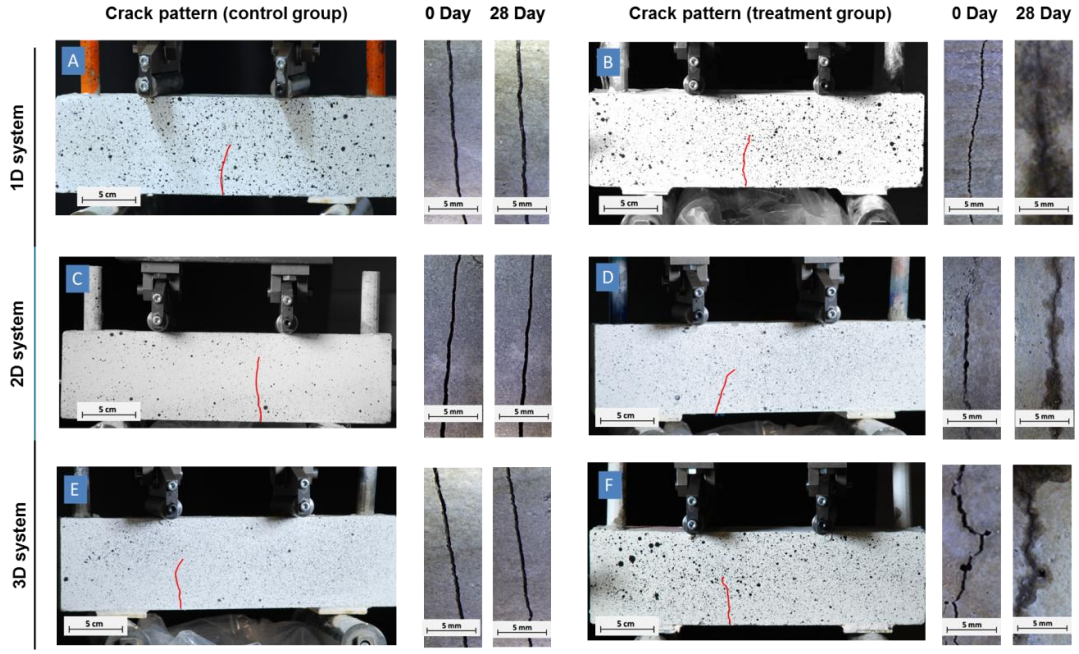

Figure 10. Photography of vascular beam crack pattern and microscope images of the main crack healing process in three different vascular systems after first Four-point bending test; controlled group (without healing agent) A, C and E; treatment group (with healing agent pumping) B, D and F.

After 28 days of pumping sodium silicate, a dark area around the cracks showed fresh healing agents were filling in cracks in all vascular systems. In most of microscope images, solidified gels were then found both inside and around crack systems after 28 days due to long term pumping (Figure 10). No crack closure was observed in all controlled samples, as a crack width around 0.7 mm is too large for autogenous self-healing.

Crack widths before and after 28 days healing are plotted in the diagram in Figure 11. In Figure 11 A, the yellow area illustrates the region covered by the plotting the crack width after 28 days versus the original crack for the control samples (1D/2D/3D) without healing agents pumped in. This indicates that there was few crack closure observed after autogenous healing process exposed in air. However, this case changed after healing. The grey area in Figure 11 B illustrated for the 1D vascular-cement system. The upper boundary of the grey area correlates with unhealed cracks and indicates cracks with none and/or little crack width reduction in 28 days. At the same time, the lower boundary of the grey area indicates cracks with significant reduction

in width due to the deposition of healing products. For the 1D vascular-cement system, the wide range of data indicating healed and unhealed cracks was attributed to single-sourced distribution of the healing agent. Once the crack part near to the tube area was healed, it stopped the healing agent distribution to the further crack surface. Alternatively, the 2D vascular-cement system, represented by the red area, shows a drop in the upper boundary, indicating an increased crack healing efficiency. The lack of variation for the 3D-vascular cement system is indicated by the narrow blue area, thus demonstrating that most of the cracks were healed after 28 days. In this case, the vascular pumping system has significantly improved the healing potential and could heal cracks with widths of around 700 μm.

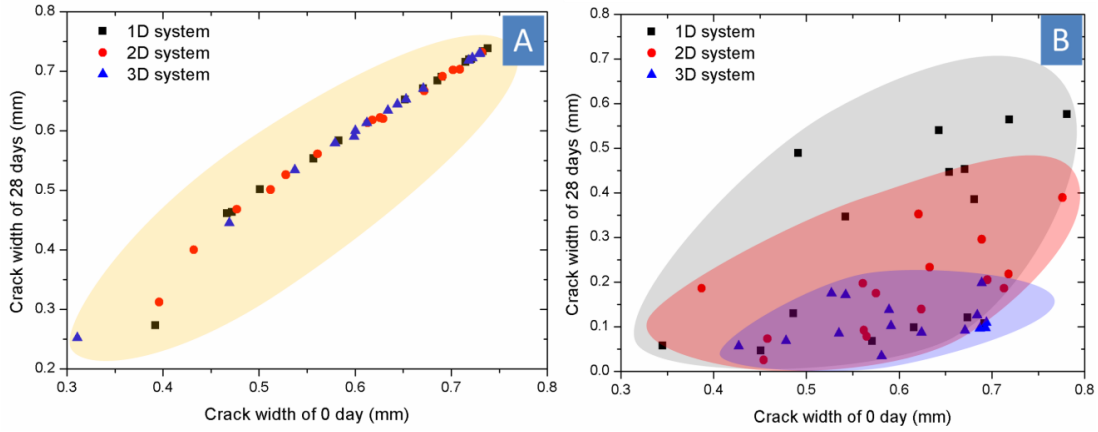

Figure 11, Crack closure diagram of 1D/2D/3D vascular systems control group (A) and treatment group (B) before and after 28 days of healing

The healing performance showed increasing trend with an increasing dimensions of vascular designs. Quantitatively, crack closure rate from microscope images was evaluated by the percentage of healing area closure (CA, %) using the following equation:

$$\mathrm{CA}(\%) = \frac{CA_0 - CA_t}{CA_0} \times 100\% \qquad (3.9)$$

Where CA_0 (mm^2) is the crack cross-section area after cracking and CA_t (mm^2) is the crack cross-section area after healing time *t*. Here in this early test, data were only collected after 28 days of healing. The crack cross-section areas were calculated via Image J software. The closure percentages of 3D vascular specimens were up to 81%, followed by the 2D system, at around 69%. 1D system held the lowest closure percentage, at around 52%. This cannot be significantly improved by extending pumping time, as the healed part of the crack would block further healing agent release from tubes. A previous investigation on 1D and 2D vascular-cement systems revealed a ~45% crack closure for 1D systems and ~72% when more parallel tubes were added when a similar mineral healing agent was used (Heywood, 2015). This indicates the importance of multiple sources of healing agent delivered at the crack surface by the vascular network on enhancing the crack closure efficiency.

Gel liked healing product was found in all three systems. The SEM

characterisation of the healing products, after the sodium silicate was delivered using a vascular network, shows the presence of plate-shaped materials. EDX analyses conducted on them revealed that the product consists mainly of O (44.87 wt%), Na (41.72 wt%), Si (10.42 wt%) and C (3.00 wt%) elements. These elements were attributed to the reaction between Na_2SiO_3 and CO_2 (air) in the presence of water vapour at temperatures at low temperature (<60 °C) (Rodríguez-Mosqueda and Pfeiffer, 2013):

$$Na_2SiO_3 + 2CO_{2(g)} + H_2O_{(v)} \rightarrow 2Na_2HCO_3 + SiO_2 \quad (3.10)$$

This explains the presence of carbon in solidified gel materials. And the crystallinity of Na_2HCO_3 at 25 °C is also plate-shaped as shown in Figure 12. However, silica was not found under the SEM image, as silica was generated in the amorphous phase in long-term and at low-temperature condition (Bettermann, 1975). This healing material is different compared to calcium-silicate-hydrate and calcium hydroxide reported by Giannaros et al. (2016) and Kanellopoulos et al. (2015). The difference was attributed to the pumping system for all vascular networks providing excessive sodium silicate. Most of them were exposed to air and reacted with CO_2 and water vapour, thereby forming the glue-like Na_2HCO_3 and silica mixed gel.

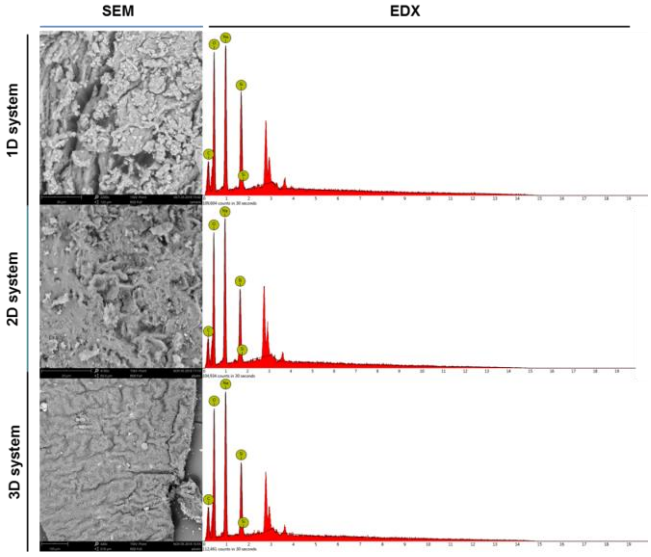

Figure 12, SEM/EDX morphology and elemental analysis of infill materials in cracks after 28 days of healing in 1D/2D/3D vascular systems

3.5 Computed tomography reconstruction

CT-scan was used to obtain 3D maps of the internal infrastructure indicating the healing agent distribution and the relationship between vascular tubing designs and crack healing area. It revealed that in both 1D and 2D systems, only the cracking area below and around tubes were healed, as shown from the reconstructed cross-section diagrams in Figure 13. As for the 3D vascular specimen, crack successfully triggered 6 tubes (out of 8), which all released sodium silicate gels to the crack, covering most of the cracking area. On the top of Figure 13, the grey level images of specimens incorporating 1D/2D/3D vascular networks reflected the density and elements atomic

number of different materials (cement, light grey; gel & healed cracks, grey; PLA, dark grey; cracks & bubbles, black). Cement, gels, tubes and empty space volume were then separated and calculated by using Mimic software and reconstructed in a three-dimensional images showed in the bottom of Figure 13. The volume fractions of PLA presented were similar in 1D/2D/3D systems (1D: 2.24%; 2D: 2.42%; 3D: 2.38%), which indicated that the increasing loading trend is mainly related with geometry shape rather than PLA volume fractions.

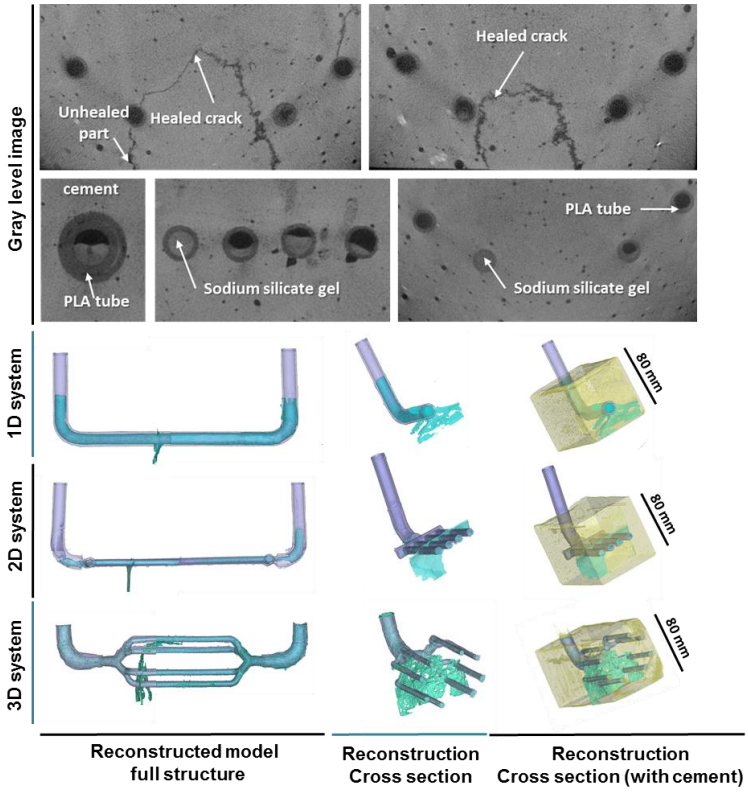

Figure 13, CT gray level image and reconstructed image of 1D/2D/3D vascular specimens, where the yellow coloured part represents cement beam; violet coloured part represents PLA vascular structure; blue coloured part represents sodium silicate gels; light blue (1D/2D) /green (3D) coloured part represents gels filled in crack

Here we adapted Shim et al (2018) the definition describing crack healing ratio (H_r), by comparing origin crack volume before healing percentage (V_{crack}, mm^3) with the percentage of gels healing volume (V_{gel}, mm^3) from CT reconstructed model as:

$$H_r = \frac{V_{gel}}{V_{crack}} \quad (3.11)$$

The healing ratio of 3D vascular specimens was around 72%, which is followed by 49% in the 2D system. The lowest healing ratio was observed in 1D system, at around 36%. This shared a similar trend with crack closure percentage data, suggesting that 3D vascular system had sufficiently covered the cracking area and had the best healing ratio compared with that in 1D and 2D systems. The increased crack healing ratio in the 3D vascular-cement systems contributed to the improvement in the load recovery of the specimens, where the 3D vascular beam reached 34% after

546 healing and positively correlated with water tightness.

547 The diffusion distance from the tubing to the cracks varied in different systems.
548 The healing agent needed to travel 36 mm (maximum) to reach the cracking area in
549 1D system, which significantly reduced the healing efficiency. In the 2D system, the
550 maximum distance of the diffusion path reduced to around 28 mm, due to a larger
551 tube coverage. This figure was again decreased to 21 mm in the 3D system, owing to
552 its highly connected network and large tube coverage.

553 The delivery of healing agents to the crack using vascular network relies on a
554 two-step process: first the sodium silicate was delivered into the crack surface, where
555 the main distribution forces were the pumping and gravity. After the solidification of
556 the sodium silicate, the healing products were deposited around the vascular tube,
557 minimising the dripping of healing agent but also decreasing the spreading around the
558 crack surface. As a result, only partial healing occurred within the crack, even after 28
559 days of pumping healing agent. The partial healing is most pronounced in the 1D- and
560 2D-vascular cement system, where the tubes were positioned below the central crack
561 zone, resulting mostly in healing around the tube and at the crack mouth. In addition,
562 at a crack width of 700-800 µm, the capillary force is not strong enough to drive the
563 healing agent up and fill in the crack tip (Thao, 2011). As a result, both 1D and 2D
564 system failed to deliver healing agents in the crack tip area, as shown in Figure 16.
565 Similar results were also found in Heywood (2015), reporting 38% and 60% of crack
566 area, was covered by 1D and 2D systems, respectively; and the crack tip zones were
567 not covered by any healing agents. In contrast, the 3D-vascular cement system
568 provides multiple sources of healing agent to the crack surface, maximising the
569 delivery of healing agent before the solidification of the sodium silicate heals the area
570 around the tube.

571 The distribution of healing agent using the 1D, 2D and 3D-vascular cement
572 system is schematically represented in Figure 14. For the 1D-vascular cement system,
573 most of the crack mouth is filled in with healing agents since the capillary force is not
574 strong enough to suck healing agent to fulfil the above space. This fulfil area is also
575 limited by continuous healing agent supply, as sealed crack mouth would block
576 further agent supply. Thus healing area in regime 1 is only located around the tube.
577 Similar scenario is found in regime 2 (Figure 14 B), healing area is also restricted
578 around crack mouth. While, parallel interconnected tubes enable larger tube coverage
579 in crack plate, providing alternative channels for healing agents to travel to the crack
580 area, thereby enlarging healing area at crack mouth zone. In regime 3 (Figure 14 C), a
581 3D vascular network is designed to provide more tube coverage at crack plate
582 compared with 1D and 2D structures. Single tube (1D) or paralleled tubes (2D) were
583 restricted by their geometry shapes to increase their tube coverage at crack section. As
584 they cannot unlimitedly enlarge their volume to increase tube coverage by weakening
585 cement matrix. To achieve large tube coverage area at crack section, branching tubes
586 should be assigned in three dimensions.

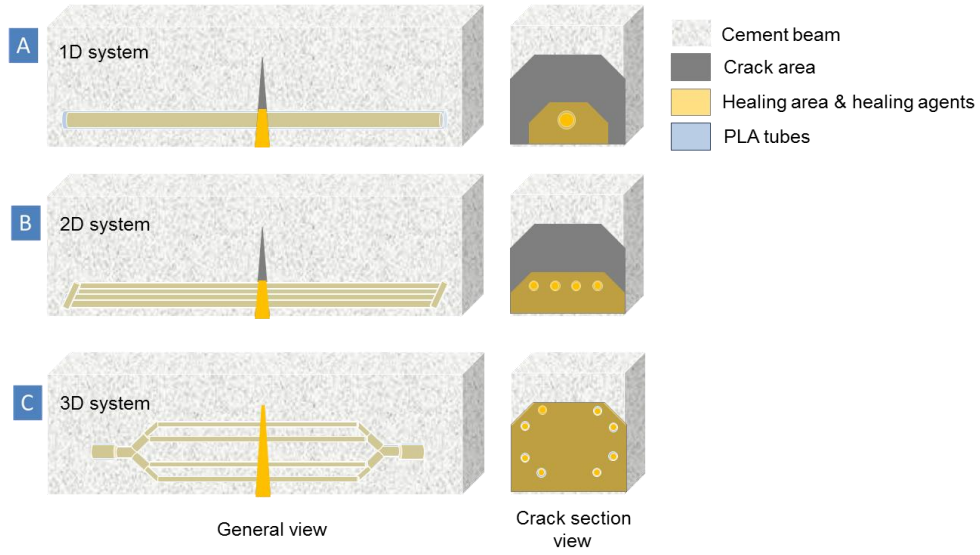

Figure 14 Healing regimes and applications in 1D (A), 2D (B) and 3D (C) systems

Upper branching tubes above the tension zone perfectly solve the problem of insufficient capillary forces, ensuring healing agents filling in both crack mouth and tip zone. 3D vascular network has a shorter diffusion path (from the PLA tubing to the cracks), by having a larger tube coverage in the cement matrix compared with the 1D and 2D systems. This significantly improved the healing performance. 8 alternative channels secure continuous healing agent supply during the period of healing. This 3D design resulted in a 72% of healing ratio compared with 36% and 49% in 1D and 2D systems. This suggested that partial healing could be drastically reduced by applying a 3D vascular structure, which contains more connected daughter tubes and enable large tube coverage. This is because an increase in several interconnected tubes could ensure healing agents supply since more alternative options are provided for agents to reach cracking area over time. Besides, larger tube coverage area in crack section solves the problem when capillary force is not strong enough to absorb healing agents to crack tip from tension zone.

4. Conclusions

For the first time, a 3D-vascular network based on a biomimetic design that follows Murray's Law was developed, 3D-printed and compared with corresponding 1D and 2D networks for use in self-healing of cementitious materials. Murray's law was obeyed during the design of the 3D-vascular network, aiming at minimising turbulent flow at junctions while also broadening distribution of healing agents. 3D printed structures presented brittle fractural response and suitable interfacial bond for mechanical triggering. Besides, the increased load applied to crack the samples with embedded 1D, 2D and 3D vascular network indicated that the plastic tube acted as a reinforcement of the cement beams. The vascular network was effective in delivering the pumped sodium silicate as a healing agent for 28 days in the three systems. Initial cracks (between 700 to 800 μm) from all systems were observed to be healed after 28 days. A recovery in mechanical properties of ~20% for 1D and 2D-structures and 34% for 3D vascular network specimens were attributed to self-healing. Additionally, the

inclusion of 1D, 2D and 3D vascular network led to around 25, 69 and 77% reduction in sorptivity in comparison with the values of the cracked control specimens. An increased amount of crack healing was observed in the 2D vascular-cement system compared with the 1D system, and nearly all the crack were reduced in the 3D vascular-cement system. Through SEM-EDX, Na2HCO3 and silica mixed gel were found as healing products as the sodium silicate was exposed to air and reacted with CO2 and water vapour. The healed crack volume was investigated by CT-scanning and indicated partial healing could be drastically reduced by applying a 3D vascular structure, which contains more connected daughter tubes and enables large tube coverage. The systematic improvement in the healing performance of the 3D vascular network specimens was attributed to the design obeying Murray's law and therefore broadening the coverage of healing agent distribution while reducing the energy required for pumping.

Acknowledgments

Support from the UK Engineering and Physical Sciences Research Council (EPSRC) for the programme grant Resilient Materials for Life (EP/02081X/1, 2017–2022) is gratefully acknowledged. Many thanks to Chris Knight for technical supports and Keturah Smithson for carrying out the CT scanning tests.

Data availability

The raw data required to reproduce these findings are available to download from: https://doi.org/10.17863/CAM.45292

References

Akers A., Gassman M., and Smith R., Hydraulic Power System Analysis (CRC, Florida, 2006).

Alghamri, R.; Kanellopoulos, A.; Al-Tabbaa, A. Impregnation and encapsulation of lightweight aggregates for self-healing concrete. Constr. Build. Mater. 2016, 124, 910–921.

Bejan, A., 1996. Street network theory of organization in nature. J. Adv. Transportation 30, 85-107.

Bettermann, P. 1975. The transformation of amorphous silica to crystalline silica under hydrothermal conditions. Contributions to Mineralogy and Petrology. Volume 53, Issue 1, pp 25–36.

Choi, S., Lee, M. G., & Park, J. K. 2010. Microfluidic parallel circuit for measurement of hydraulic resistance. Biomicrofluidics, 4(3), 034110.

Davies, R., Jefferson, A., Lark, R., Gardner, D. A Noval 2D Vascular network in cementitious materials. Concrete – Innovation and Design, fib Symposium, Copenhagen May 18-20, 2015

Dry, C. M. 1994. Matrix cracking repair and filling using active and passive modes for smart timed release of chemicals from fibers into cement matrices. Smart Mater.

Struct. 3, 118–123.Davies, R., Jefferson, A., Lark, R., Gardner, D. A Noval 2D Vascular network in cementitious materials. Concrete – Innovation and Design, fib Symposium, Copenhagen May 18-20, 2015

De Belie, N., Gruyaert, E., Al-Tabbaa, A., Antonaci, P., Baera, C., Bajare, D., Darquennes, A., Davies, R., Ferrara, L., Jefferson, T., Litina, C., Miljevic, B., Otlewska, A., Ranogajec, J., Roig-Flores, M., Pain, K., Lukowski, P., Serna, P., Tulliani, J. M., Vucetic, S., Wang, J., Jonkers, H.M. A review of self-healing concrete for damage management of structures. Adv. Mater. Interfaces, 5 (17) (2018), pp. 1-28

De Rooij, M., Van Tittelboom, K., De Belie, N., Schlangen, E., 2013. State-of-the-Art Report of RILEM Technical Committee 221-SHC: Self-Healing Phenomena in Cement-Based Materials, page 8-12.

Formia, A., Terranova, S., Antonaci, P., Pugno, N., Tulliani, J. 2015 Setup of extruded cementitious hollow tubes as containing/releasing devices in self-healing systems Materials 8 1897–923.

Giannaros, P., Kanellopoulos, A., Al-Tabbaa, A. 2016. Sealing of cracks in cement using microencapsulated sodium silicate. Smart Materials and Structures, 25.084005 (12pp).

Günaydın, K., Türkmen, H. S., 2018. Common FDM 3D Printing defects. International Congress on 3D Printing (Additive Manufacturing) Technologies and Digital Industry Conference.

Hall, C. and Tse, T. K. M., 1986. Water movement in porous building materials-VII. The sorptivity of mortars. Building and Environment, 21(2), 113-118.

Heywood, D. 2015. Biomimetic Vascular Networks for Self-Healing Concrete. CUED.

Huang, H., Ye, G., Shui, Z. 2014. Feasibility of self-healing in cementitious materials – By using capsules or a vascular system? Construction and Building Materials, Volume 63, Pages 108-118.

Joseph C, Jefferson AD, Isaacs B, Lark R, Gardner D. 2010. Experimental investigation of adhesive-based self-healing of cementitious materials. Magazine of Concrete Research, 62, No. 11, November, p.831–843.

Justin, A. W., Brooks, R. A., Markaki, A. E. 2016. Multi-casting approach for vascular networks in cellularized hydrogels, J. R. Soc. Interface 13: 20160768.

Kanellopoulos, A., Qureshi, T.S., Al-Tabbaa, A. 2015. Glass encapsulated minerals for self-healing in cement based composites. Construction and Building Materials, Vol. 98, 780-791.

Kim, B. and Han, Y., 2017. Flexural performance of transparent plastic bar Reinforced concrete. Applied Sciences. 2018, 8, 325.

694 Kimber, C. Biomimetic vascular networks for self-healing concrete. CUED, 2014.

695 Lim, D., Kamotani, Y., Cho, B., Mazumder, J., Takayama, S. 2003. Lab on a Chip -
696 Miniaturisation for Chemistry and Biology 3, 318–323.

697 Miguel, A. F., 2016. Toward an optimal design principle in symmetric and asymmetric
698 tree flow networks. Journal of theoretical biology, 389, 101-109.

699 Minnebo, P., Thierens, G., de Valck, G., van Tittelboom, K., de Belie, N., van
700 Hemelrijck, D., Tsangouri, E. A novel design of autonomously healed concrete:
701 towards a vascular healing network. Materials. 2017, 10, 49, 1-23.

702 Murray, C. D. 1926a. The physiological principle of minimum work applied to the
703 angle branching of arteries, Proc. Nat. Acad.Sc., xii, 207, 835-841.

704 Murray, C. D. 1926b. The physiological principle of minimum work—I: The vascular
705 system and the cost of blood volume. Proc. Natl. Acad. Sci., 12, 207–214.Sangadji,
706 S. 2017. Can self-healing mechanism helps concrete structures sustainable?
707 Procedia Engineering 171, 238-249.

708 Oropallo, W., Pieg, L.A., 2016. Ten challenges in 3D printing. Engineering with
709 Computers, 32, 135–148.

710 Razavi, M. S., Shirani, E., Salimpour, M. R. 2014. Development of a general method
711 for obtaining the geometry of microfluidic networks, AIP Advances 4, 017109.

712 Rodbard, S., 1975. Vascularcaliber.Cardiology. 60, 4–49.

713 Rodríguez-Mosqueda, R. and Pfeiffer, Heriberto. 2013. High CO_2 Capture in Sodium
714 Metasilicate (Na_2SiO_3) at Low Temperatures (30–60 °C) through the CO_2–H_2O
715 Chemisorption Process. The Journal of Physical Chemistry C, 117 (26),
716 13452-13461.

717 Shim, Y., Hong, G., Choi, S. 2018. Autogenous healing of early-age cementitious
718 materials incorporating superabsorbent polymers exposed to wet/dry cycles.
719 Materials 2018, 11, 2476.

720 Thao, T.D.P. 2011. "Quasi-Brittle Self-Healing Materials: Numerical Modelling and
721 Applications in Civil Engineering." PhD Thesis, National Unviersity of Singapore.

722 Van Tittelboom, K. de Belie, N., van Loo, D., Jacobs, P. Self-healing efficiency of
723 cementitious materials containing tubular capsules filled with healing agent. Cem.
724 Concr. Compos. 2011, 33, 497-505.

725 Van Tittelboom, K. and De Belie, N. 2013. Self-Healing in Cementitious
726 Materials—A Review. Materials 2013, 6, 2182-2217.

727 Wegst, U. G. K., Bai, H., Saiz, E., Tomsia, A. P., Ritchie, R. O., 2015. Bioinspired
728 structural materials. Nature Materials, Vol. 14, 23–36.

729 Williams, H. R., Trask, R. S., Knights, A. C., Williams, E. R. Bond, I. P. 2008.
730 Biomimetic reliability strategies for self-healing vascular networks in engineering

731 materials. J. R. Soc. Interface, 5, 735–747.

732 Yuhazri, M. Y., Hafiz, K.M., Myia, Y. Z. A., Jia, C. P., Sihombing, H., Sapuan, S. M.,
733 Badarulzaman, N. A., 2017. The Effect of Different Shape and Perforated rHDPE in
734 Concrete Structures on Flexural Strength. IOP Conf. Series: Journal of Physics:
735 Conf. Series 914 (2017) 012023.

736 Zhou, X., Hsieh, S., Ting, C., 2018. Modelling and estimation of tensile behaviour of
737 polylactic acid parts manufactured by fused deposition modelling using finite
738 element analysis and knowledge-based library. Virtual and Physical Prototyping,
739 13(3), pp.177-190.